A Doubly Adaptive Approach to Dynamic MRI Sequence Estimation

William Scott Hoge, *Member, IEEE*, Eric L. Miller, *Member, IEEE*, Hanoch Lev-Ari, *Senior Member, IEEE*, Dana H. Brooks, *Member, IEEE*, and Lawrence P. Panych

***Abstract*—Dynamic magnetic resonance imaging (MRI) refers to the acquisition of a sequence of MRI images to monitor temporal changes in tissue structure. In this paper we present a method for the estimation of dynamic MRI sequences based on two complimentary strategies: an adaptive framework for the estimation of the MRI images themselves, and an adaptive method to tailor the MRI system excitations for each data acquisition. We refer to this method as the *doubly adaptive temporal update method* (DATUM) for dynamic MRI.**

Analysis of the adaptive image estimate framework shows that calculating the optimal system excitations for each new image requires complete knowledge of the next image in the sequence. Since this is not realizable, we introduce a linear predictor to aid in determining appropriate excitations. Simulated examples using real MRI data are included to illustrate that the doubly adaptive strategy can provide estimates with lower steady state error than previously proposed methods and also the ability to recover from dramatic changes in the image sequence.

***Index Terms*—Adaptive filters, dynamic MRI, image tracking, minimum data MR image reconstruction, SVD.**

I. Introduction

MAGNETIC resonance imaging (MRI) has rapidly become the imaging modality of choice for noninvasively acquiring high-resolution images of soft tissue. One application of MRI is to monitor dynamic changes in tissue structure through the acquisition of a sequence of images focused on the same slice or region of tissue over a period of time. Clinical applications where dynamic MRI is of interest include the observation of the early flow of contrast agent to detect and localize tumors [1], [2], real time monitoring of surgical interventions or thermal treatments [3], and cardiac imaging [4]. Because of fundamental limits in the MRI data acquisition rate, there is a tradeoff in each of these cases between temporal resolution, spatial resolution, volume coverage and signal-to-noise ratio. For example, the ability to image cardiac activity in real time comes at the expense of limited volume coverage and low spatial resolution [5]. Thus, there is a need for optimized data acquisition that allows for faster image sequence reconstruction using a limited amount of acquired data.

Traditional MRI acquisition techniques use magnetic field gradients and radio-frequency (rf) pulses to encode the spatial position of different particles within a tissue volume. The input system excitations of gradient fields and rf pulses are used to scan a volume in a sequence of slices, typically via direct sampling of the two-dimensional spatial Fourier encoding, or k-space, of the slice. An inverse Fourier transform is then used to reconstruct images of the tissue composition. Good reviews of this process from a signal processing perspective are available in [6] and [7].

The physical dynamics of MR imaging constrain the image acquisition time. Typically, one line in k-space is sampled for each input excitation. For a static image slice, one can improve the spatial resolution by increasing both the number of sampled k-space lines and the bandwidth of k-space they cover. However, when the composition of the slice changes over time, only the most recently acquired data accurately reflects the present composition of the slice and the oldest acquired data may not be reliable. Thus the challenge of improving temporal resolution of an image sequence is not directly analogous to increasing spatial resolution.

One approach to improve the spatial and temporal resolution of an acquired image sequence is to acquire a multiple number of sampled k-space lines per input excitation. However, such *multiline* techniques typically require enhanced hardware to implement and suffer more from image distortion and artifact. For example, echo-planar imaging (EPI) samples a cyclic raster line through k-space, but requires quickly switching a strong magnetic gradient field [8, p. 152]. Alternatively, *parallel imaging* methods such as SMASH [9] use a phased array of receiver coils to rapidly sample different segments of k-space concurrently. Such methods represent a *hardware* solution to the problem.

We consider in this paper a complementary *software* approach. Under the assumption that one line of k-space is acquired with each input excitation, the required image acquisition time is proportional to the number of lines sampled in k-space, or equivalently, the number of excitations used. It follows that the dynamic sequence acquisition time can be reduced—and the temporal resolution improved—by reducing the number of input excitations employed. The underlying images are then estimated using a minimal amount of acquired data. The challenge is to identify and acquire "enough" useful data to accurately estimate the sequence images while at the same time limiting the amount of acquired data. As we demonstrate in this paper, this translates to the identification of an appropriate acquisition subspace tailored to minimize the image sequence tracking error.

Manuscript received October 22, 2001; revised July 1, 2002. This work was supported under NSF CAREER Grant MIP-9623721, and was supported in part by CenSSIS, the Center for Subsurface Sensing and Imaging Systems, under the Engineering Research Centers Program of the National Science Foundation under Award EEC-9986821, and NIH T32 Training Grant PA-103-AA. The associate editor coordinating the review of this manuscript and approving it for publication was Dr. Mark R. Luettgen.

W. S. Hoge and L. P. Panych are with the Department of Radiology, Harvard Medical School and Brigham and Women's Hospital, Boston, MA 02115 USA (e-mail: shoge@ieee.org).

E. L. Miller, H. Lev-Ari, and D. H. Brooks are with the Department of Electrical and Computer Engineering, Northeastern University, Boston, MA 02215 USA.

Digital Object Identifier 10.1109/TIP.2002.804272.

1057-7149/02$17.00 © 2002 IEEE

Previous MRI sequence estimation methods using minimal data acquisition follow one of two general system excitation approaches. The first defines a set of static excitations, using no information about the underlying image. Here, the physical MRI acquisition process suggests using a truncated Fourier basis set. Such techniques include the Fourier keyhole (FK) method [10], RIGR [11], and the multiple region MRI method [12]. Predefined non-Fourier excitations have also been proposed, such as the wavelet techniques in [13] and [14]. The second approach is to generate a static excitation set based on some known information about the image obtained from a previously acquired data set. For example, a full image scan may be obtained just before the introduction of contrast agent or prior to surgical intervention. Information from this full image can then be used to design excitation sequences to efficiently acquire subsequent image data in the dynamic sequence. One such method is to construct excitation sequences using information from the singular value decomposition (SVD) of a given reference image [15]. Such methods can be considered complementary to the hardware techniques mentioned earlier. For example, combined SVD and EPI methods have been demonstrated [16] as well as multiline SVD acquisition techniques [17].

To estimate the image sequence, each of the acquisition methods cited above uses a given set of system excitations, recorded output data, and an image reconstruction model. Utilizing a set of static input excitations, they are adaptive in the sense that each new image estimate is constructed from some prior knowledge plus an update term utilizing the most recently recorded output data. However, due to the dynamic nature of MRI sequences, a static excitation set—either Fourier or non-Fourier based—may not be best over an entire sequence. A variety of input selection methods been proposed [12], [18], [19], but here we seek to adaptively determine the input excitation sequences as well, making the problem of dynamic MR image sequence estimation *doubly adaptive*.

The challenge is that only the current input excitation and output measurements are available for determination of both the image estimate and the next set of system inputs. Furthermore, much like the classic "Which came first, the chicken or the egg" paradox, the resulting quality of each half of the doubly adaptive system depends directly on the other.

This paper presents our doubly adaptive temporal update method (DATUM) as a solution to this problem. The DATUM solution builds upon the linear system model given by Panych *et al.* in [20], which we briefly review in Section II. This system model is applicable to both Fourier and non-Fourier encoding techniques. However, realization of the advantages provided by non-Fourier encoding—and the DATUM method in particular—brings with it a number of research questions that are detailed in Section VI, but lie beyond the scope of this paper. In Section III, we develop a general image estimation framework where we follow a traditional adaptive filtering approach, minimizing a measure of the difference between the measured system response and the expected output data. Analysis of this framework, presented in Section III-C, shows that the FK and SVD methods previously proposed are in fact specific cases of this adaptive framework.

Section III-D presents an analysis of the estimate error for the adaptive framework developed in Section III-C. This analysis reveals that the identification of the theoretically optimal input excitation sequence requires complete knowledge of the next image in the sequence, regardless of the image reconstruction method. Because this information is not available in a clinical setting, Section IV presents a realizable method to bypass this limitation. Specifically, we propose using a linear predictor in tandem with, but distinct from, the image sequence estimation. This enables the use of a predicted estimate of the next image in the sequence to tailor an appropriate set of system excitation inputs.

A comparison between the DATUM methods presented in this paper and the minimal data imaging methods developed previously is given in Section V. The examples show simulations of a dynamic MRI sequence acquisition, utilizing real MRI data, for the FK, SVD, RIGR, and the DATUM methods. As illustrated in Section V, the DATUM methods produce a sequence estimate with lower steady state error than previous methods, and is applicable for estimating dynamic MRI sequences that exhibit bulk motion changes.

II. Linear System Model for MRI

The DATUM methods presented in this paper build on the linear system model developed by Panych *et al.* [20]. The following section presents a brief review of this MRI acquisition model. In general, the MRI system mapping from input excitation to sampled output data is nonlinear. However, if the acquisition uses rf encoding with a low flip angle excitation, the MRI system input–output mapping may be approximated to the first order and the MR imaging process can be described by a linear response model [20].

In this paper, we refer to each rf excitation as an input and each measured rf signal as a system output. The time samples of an rf excitation are denoted with an input vector $\mathbf{x}_i$. Similarly, the vector $\mathbf{y}_i$ represents time samples of the measured rf signal envelope. If we represent the k-space encoding of a given image slice with the matrix $\mathcal{R}$, then the MRI data acquisition process may be modeled with a matrix–vector product, $\mathbf{y}_i = \mathcal{R}\mathbf{x}_i$.

Typically, one collects r such scans together to form the matrix equation $\mathcal{Y} = \mathcal{R}\mathcal{X}$, where $\mathcal{R}$ is a data matrix of size $M \times N$ that characterizes the system response, $\mathcal{X}$ is an $N \times r$ matrix constructed from the input vectors $\mathcal{X} = [\mathbf{x}_1 \quad \mathbf{x}_2 \quad \cdots \quad \mathbf{x}_r]$, and $\mathcal{Y}$ is an $M \times r$ matrix constructed from the output vectors, $\mathcal{Y} = [\mathbf{y}_1 \quad \mathbf{y}_2 \quad \cdots \quad \mathbf{y}_r]$. The line-by-line acquisition of the k-space data for a given image slice would be represented by $\mathcal{X}$ equal to an identity matrix of size $N \times N$. For minimal data acquisitions, the goal is to set $r \ll N$ and still provide high-quality estimates of $\mathcal{R}$.

If one includes additive noise, $\mathcal{N}$, then a more general acquisition model can be written as $\mathcal{Y} = \mathcal{R}\mathcal{X} + \mathcal{N}$. If the noise is independent and identically distributed, then it can be shown (e.g., [21]) that with orthogonal inputs vectors, the least-squares estimate of the system response matrix is $\hat{\mathcal{R}} = \mathcal{Y}\mathcal{X}^{\dagger}$ where $X^{\dagger}$ denotes the pseudo-inverse of $\mathcal{X}$. This result is identical to the noise-free case we develop below. Thus, in this paper we impose the constraint of orthogonal input vectors, and proceed below using the noise-free acquisition model.

For dynamic sequences, $\mathcal{R}$ varies in time. For the analysis that follows below, we assume that the data matrix $\mathcal{R}$ changes

smoothly and that any change occurs much more slowly than the time to acquire r scans. Specifically, if $\Delta\mathcal{R}$ represents the change in the image data during r scans, then we assume that $||\Delta\mathcal{R}||_F^2 \ll ||\mathcal{R}||_F^2$.

For convenience, here we choose to transform the measured k-space domain output data to the spatial domain by defining the $N \times N$ unitary Fourier transform matrix [22, Ch. 5]: $F_N = \{(N)^{-1/2} e^{-j2\pi kn/N}\}$, $0 \le k, n \le N-1$. This allows one to transform the sampled k-space data matrix $\mathcal{R}$ to the spatial domain via $A = F_M^H \mathcal{R} F_N$. To view the image, one typically displays the magnitude of this matrix, $|A|$. The motivation for this transformation choice, as opposed to the standard 2D Fourier transform $F_M \mathcal{R} F_N$, is that the k-space excitation and output vectors can be transformed to the spatial domain in an identical way, via $X = F_N^H \mathcal{X}$ and $Y = F_M^H \mathcal{Y}$.

For the remainder of this paper, we choose to work entirely in the spatial image domain. The linear model we use is

$$Y_n = A_n X_n \tag{1}$$

where the subscript n refers to the image frame number in the acquired dynamic sequence, A_n is the $M \times N$ image at time n, X_n is a block of input rf excitations of size $N \times r$, and Y_n is a block of measured output data of size $M \times r$. Here, r refers to the number of scans used for each image acquisition and is typically less than N.

A number of MRI modalities can be represented by this model. For the wavelet and SVD methods the input vectors are static over the sequence, i.e., $X_n = X$, and are chosen from either a pre-selected wavelet basis [13] or from the r dominant right singular vectors of a reference image matrix A_0 [15], [23]. The image estimates are constructed via

$$\hat{A}_n = Y_n X^H = A_n X X^H. \tag{2}$$

For the FK method [10], the static input rf excitation matrix, $X_n = X$, captures the lower spatial frequency components of k-space. The acquired data then replaces a portion of the k-space data in the current estimate. This can be represented analytically as

$$\hat{A}_n = A_n X X^H + A_0\big(I - X X^H\big) \tag{3}$$

where A_0 is again a reference image data matrix and I is the identity matrix of size $N \times N$. If X is chosen as the dominant right singular vectors of A_0 instead, then (3) represents the keyhole variant of the SVD method described in [24].

The key advantage of these methods is that one can easily generate an estimate $\hat{A}_n$ of the image slice at time n using a limited amount of new data. That is, useful image representations are available even if one uses $r < N$ excitation and reconstruction vectors. We note that both the FK and SVD methods assume the input vector set X is formed from orthonormal columns, i.e., $X^H X = I$ where I is the identity matrix. We will constrain all input excitation matrices X_n in this same manner throughout this paper.

Considering the two image sequence estimate methods presented in this section, we pose two complementary questions. First, what is the best way to form the image estimate? And second, what are the best input vectors to use? We present separate analytical approaches to these two questions in the next two sections. Specifically, Section III describes image estimation via cost function minimization for a given set of input vectors. Section IV considers the design of an effective set of input vectors based on a past history of previous image estimates. Together, these two sections comprise our DATUM MRI sequence estimator.

III. An Adaptive Framework for Image Estimation

Presented below is the analysis and solution to the first half of the doubly adaptive problem. In this section we present an approach to MR image estimation from a purely analytical perspective, drawing primarily from adaptive filter theory. Specifically, given a set of input vectors X_n we wish to estimate the image at time n through the minimization of the cost function, $\mathcal{J}_n = ||Y_n - \hat{Y}_n||_F^2$. Here, as given in (1), $Y_n = A_n X_n$ is the output data from the r scans represented in X_n, while $\hat{Y}_n = \hat{A}_n X_n$ is the expected output determined via a dynamic system estimate $\hat{A}_n$ using the same input vectors.

In the adaptive filter literature, $\mathcal{J}_n$ is often referred to as the *output error*. A more direct measure of the image reconstruction is the model *estimate error*, $\mathcal{E}_n = ||A_n - \hat{A}_n||_F^2$. However, $\mathcal{E}_n$ cannot be used to identify $\hat{A}_n$ because knowledge of A_n is not directly available. The estimate error can be used in simulations for post factum comparison of different estimate methods, as will be demonstrated in Section III-D. We also use it in Section IV to guide the identification of subsequent input vectors.

Because r was chosen such that $r < N$, i.e., X_n is a tall-skinny matrix, the minimization problem

$$\min_{\hat{A}_n} \mathcal{J}_n = \min_{\hat{A}_n} \left|\left| Y_n - \hat{A}_n X_n \right|\right|_F^2 \tag{4}$$

is underdetermined and an infinite number of zero-error solutions exist. Three solutions are presented below. Each solves the equation $\mathcal{J}_n = 0$ with a different model for $\hat{A}_n$.

A. Low-Rank Solution

First, with no structural constraints on $\hat{A}_n$, solving $\mathcal{J}_n = 0$ leads to the underdetermined system $\hat{A}_n X_n = Y_n$. One solution is the minimum norm least squares (min-norm LS) solution

$$\hat{A}_n = Y_n X_n^H \big(X_n X_n^H\big)^\dagger \tag{5}$$

where $B^\dagger$ represents the Moore–Penrose pseudo-inverse of a matrix B [25]. If the columns of X_n are constrained to be orthonormal, then $X_n^H (X_n X_n^H)^\dagger = X_n^H$ and (5) reduces to the *low-rank reconstruction* solution

$$\hat{A}_n = Y_n X_n^H = A_n X_n X_n^H. \tag{6}$$

This low-rank estimate was used by Panych *et al.* in the SVD encoding method [15].

B. Incorporating a Reference Image

One could instead solve $\mathcal{J}_n = 0$ while incorporating information from a reference image. Traditionally, this reference image is obtained at the start of the sequence acquisition [10], [23], [20]. To incorporate reference image information in the image

estimate, we model the image estimate as $\hat{A}_n = A_0 + \Delta_n$. Finding the min-norm LS solution for $\mathcal{J}_n = 0$ with this model for $\hat{A}_n$ gives

$$Y_n - (A_0 + \Delta_n)X_n = 0$$
$$\Delta_n = (Y_n - A_0 X_n)X_n^H \left(X_n X_n^H\right)^{\dagger}.$$

Again, with the constraint that the columns of X_n are orthonormal, this leads to

$$\begin{aligned}\hat{A}_n &= A_0 + Y_n X_n^H - A_0 X_n X_n^H \\ &= Y_n X_n^H + A_0\left(I - X_n X_n^H\right).\end{aligned} \tag{7}$$

If the inputs X_n are constructed from the low-frequency components of the Fourier basis, one can recognize (7) as the *keyhole reconstruction* method of Brummer and van Vaals *et al.* [10]. Furthermore, if $A_0 = \mathbf{0}$, then this solution is identical to the low-rank reconstruction in (6).

C. General Adaptive Framework

A third possibility is to solve $\mathcal{J}_n = 0$ while incorporating information from the most recent estimate, $\hat{A}_n = \hat{A}_{n-1} + \Delta_n$. This leads to

$$Y_n - \left(\hat{A}_{n-1} + \Delta_n\right)X_n = 0$$
$$\Delta_n = \left(Y_n - \hat{A}_{n-1}X_n\right)X_n^H \left(X_n X_n^H\right)^{\dagger}.$$

In this case, imposing the orthogonality constraint on X_n gives an *adaptive framework* solution

$$\hat{A}_n = Y_n X_n^H + \hat{A}_{n-1}\left(I - X_n X_n^H\right). \tag{8}$$

We can identify where this equation resides in the pantheon of adaptive filter theory via the following. First, for the case of $r = 1$, we can rewrite (in MATLAB-style row-major notation) each row m of the image estimate (8) as

$$\hat{A}_n(m,:) = \hat{A}_{n-1}(m,:) + \left[Y_n(m) - \hat{A}_{n-1}(m,:)X_n\right]X_n^H. \tag{9}$$

Readers familiar with adaptive filter theory may recognize this equation as the least mean square (LMS) adaptive algorithm with a step size parameter of $\mu = 1$. Furthermore, since $X_n^H X_n = I$, we can say that (9) is actually normalized LMS, with a step size parameter of $\mu = \tilde{\mu}/\|X_n\|_2 = 1$. This classification is significant because the normalized LMS algorithm is convergent in the mean square error if the adaptation constant $\tilde{\mu}$ satisfies the condition $0 < \tilde{\mu} < 2$ [26, §9.11]. For (8), the adaptation constant $\tilde{\mu}$ is equal to one and is thus convergent. Finally, for the case when $r > 1$, we note that the estimate update will occur only once for each r set of input samples. This is often referred to as *block update LMS*.

For the purpose of comparison with existing keyhole methods, consider (8) for the limiting case of a static input vector set, $X_n = X\ \forall\, n$, formed from orthonormal columns. In this case, the projection of the low-order reconstruction terms $Y_k X^H$ onto the complementary subspace $(I - XX^H)$ will result in $Y_k X^H(I - XX^H) = A_k XX^H(I - XX^H) = 0$. If in (8) we rewrite $\hat{A}_{n-1}$ in terms of $\hat{A}_{n-2}$, $\hat{A}_{n-3}$, etc., we find

$$\begin{aligned}\hat{A}_n &= Y_n X^H + \hat{A}_{n-1}\left(I - XX^H\right) \\ &= Y_n X^H + \left[Y_{n-1}X + \hat{A}_{n-2}\left(I - XX^H\right)\right]\left(I - XX^H\right) \\ &= Y_n X^H + \hat{A}_{n-2}\left(I - XX^H\right) \\ &\ \ \vdots \\ \hat{A}_n &= Y_n X^H + \hat{A}_0\left(I - XX^H\right).\end{aligned}$$

Notice that the cancellation effect occurs all the way back to the initial estimate $\hat{A}_0$. There are no contributions from the intermediate output data Y_k in the estimate of $\hat{A}_n$ for $0 < k < n$. Thus, with static orthogonal inputs, the adaptive framework solution for $\hat{A}_n$ is identical to the keyhole method described in (7) if we choose $\hat{A}_0 = A_0$. The SVD and FK methods are well known minimal data MRI acquisition techniques, although they are frequently described in the literature using the language of "data replacement." The reconstruction framework in (8) provides a common analytic framework for both methods, and potentially others as well. Because the FK and SVD methods are special cases of (8), we refer to this solution as the general adaptive estimate framework.

D. Analysis of Image Estimate Methods

Each of the above image reconstruction methods (6)–(8) are identical in terms of minimizing the output error $\mathcal{J}_n$. Specifically, $\mathcal{J}_n = \|Y_n - \hat{Y}_n\|_F^2 = 0$ for all three. If we assume, temporarily, that the entire sequence is known, then one can determine which is the best solution by comparing the image estimate $\hat{A}_n$ to the actual image A_n via the estimate error measure

$$\mathcal{E}_n = \left\|A_n - \hat{A}_n\right\|_F^2. \tag{10}$$

A summary showing the error for each of the three methods is given in Table I.

If the sequence were completely known, then Table I could be used to identify the *theoretically optimal* inputs for a given reconstruction method. Obviously, in a clinical setting the next image in the sequence is not known ahead of time, and thus the optimal input vectors implied in Table I are not directly realizable. However, they do provide a theoretical bound on the estimate quality for a given image reconstruction method.

Additionally, Table I implies that one can do better with dynamic inputs rather than static inputs as $\mathcal{E}_n$ is a function of X_n in all cases. As shown in Section IV, the minimization of $\mathcal{E}_n$ with respect to X_n provides a mechanism to determine new input vectors.

IV. System Input Vector Determination

In this section we examine the second half of the doubly adaptive problem. Specifically, we wish to determine new inputs to minimize the error in the next image estimate. For each case given in Table I, the minimization of $\mathcal{E}_n$ via a suitable choice of X_n requires a subspace identification. Specifically, the minimization of $\mathcal{E}_n$ in each of these cases is analogous to a method for the determination of the right singular vectors of a matrix. As given in [27], the maximization problem $\max_x \|Ax\|_2$ with the constraint $\|x\|_2 = 1$ will identify the

TABLE I
IMAGE RECONSTRUCTION METHOD SUMMARY SHOWING THE ESTIMATE, $\hat{A}_n$, AND THE ESTIMATE ERROR, $\mathcal{E}_n$, FOR THE LOW-RANK, KEYHOLE, AND ADAPTIVE FRAMEWORK METHODS

Method Estimate / Estimate Error
Low-rank
$\hat{A}_n = Y_n X_n^H$
$\mathcal{E}_n = \|A_n(I - X_n X_n^H)\|_F^2$
Keyhole
$\hat{A}_n = Y_n X_n^H + A_0(I - X_n X_n^H)$
$\mathcal{E}_n = \|(A_n - A_0)(I - X_n X_n^H)\|_F^2$
Adaptive Framework
$\hat{A}_n = Y_n X_n^H + \hat{A}_{n-1}(I - X_n X_n^H)$
$\mathcal{E}_n = \|(A_n - \hat{A}_{n-1})(I - X_n X_n^H)\|_F^2$

dominant right singular vector of the matrix A. From a subspace projection point of view, this is equivalent to the minimization problem $\min_x \|A(I - xx^H)\|_2$ with $\|x\|_2 = 1$.

Thus, from Table I, we find that to minimize the estimate error of the image estimate, for inputs one must use 1) the r dominant right singular vectors (rSV) of the next image for the low-rank estimate methods (6); 2) the rSV of the difference between the next image and reference image for the keyhole method (7); and 3) the rSV of the difference between the next image and current estimate for the adaptive framework estimate method (8).

Guided by this knowledge, the optimal new input vectors for the adaptive framework estimator given in (8) would be the dominant right singular vectors of $(A_{n+1} - \hat{A}_n)$. However, since A_{n+1} is unavailable, we propose replacing this term with the output of a linear predictor, denoted by $\tilde{A}_{n+1}$. Thus, we select new inputs X_{n+1} via solution of the optimization problem

$$\min_{X_{n+1}} \left\| \left(\tilde{A}_{n+1} - \hat{A}_n \right) (I - X_{n+1} X_{n+1}^H) \right\|_F^2. \tag{11}$$

A wide variety of image prediction methods are available, including temporal, spatial, and dynamic model based methods. We examine here the pixel-wise temporal predictor

$$\tilde{A}_{n+1} = \sum_{i=0}^{k-1} c_i \breve{A}_{n-i} \tag{12}$$

where $\breve{A}_n$ is the predictor input at time n and the predictor is defined by the scalar filter coefficients c_i. In the examples that follow, we construct the predicted image $\tilde{A}_{n+1}$ from a pixel-wise linear fit to k previous image estimates $\breve{A}_n, \breve{A}_{n-1}, \ldots, \breve{A}_{n-k}$. With uniform sampling in time, one can construct the closed form expression for such a predictor

$$\tilde{A}_{n+1} = \sum_{i=0}^{k-1} \left[\frac{4}{k} - i \frac{6}{k(k-1)} \right] \breve{A}_{n-i} \tag{13}$$

from the normal equations of a linear least squares fit [28, Ch. 4, §6.3], and the knowledge that $\sum_{l=0}^{t-1} l^2 = t(t-1)(2t-1)/6$ and $\sum_{l=0}^{t-1} l = t(t-1)/2$. The notation $\breve{A}_n$ was chosen in (12) to emphasize that a number of possibilities are available for the predictor input. Two choices are examined in detail below.

It is reasonable to expect that the choice of predictor input $\breve{A}_n$ affects the quality of the subsequently determined input vectors. However, the effect is nonintuitive. Consider the case of a linear predictor built from a linear temporal extrapolation of $k = 2$ images. Thus, we find $c_0 = 2$ and $c_1 = -1$ from (13), and

$$\tilde{A}_{n+1} = 2\breve{A}_n - \breve{A}_{n-1}.$$

When the predictor input is the adaptive framework estimate, namely $\breve{A}_n = Y_n X_n^H + \hat{A}_{n-1}(I - X_n X_n^H)$, we find

$$\begin{aligned} \left(\tilde{A}_{n+1} - \hat{A}_n \right) &= \left(2\hat{A}_n - \hat{A}_{n-1} \right) - \hat{A}_n = \hat{A}_n - \hat{A}_{n-1} \\ &= \left(A_n - \hat{A}_{n-1} \right) X_n X_n^H. \end{aligned} \tag{14}$$

Since the expression $X_n X_n^H$ on the right side of the matrix product expression in (14) is a subspace projection, the right singular vectors of $(\tilde{A}_{n+1} - \hat{A}_n)$ will span the same subspace as X_n. Thus, choosing new input vectors from the SVD of $(\tilde{A}_{n+1} - \hat{A}_n)$ will give vectors spanning the same subspace at every time n. We refer to this tendency as a *subspace trap*, and it is surprisingly prevalent when attempting to determine new input vectors from previous estimates [29].

As shown below, a better choice is to use the low-rank estimate as input to the predictor, namely $\breve{A}_n = Y_n X_n^H$. In this case, we find

$$\begin{aligned} \left(\tilde{A}_{n+1} - \hat{A}_n \right) &= 2Y_n X_n^H - Y_{n-1} X_{n-1}^H - \hat{A}_n \\ &= A_n X_n X_n^H - A_{n-1} X_{n-1} X_{n-1}^H \\ &\quad - \hat{A}_{n-1}(I - X_n X_n^H). \end{aligned} \tag{15}$$

Thus, by using $Y_n X_n^H$ as the predictor input, we find that the difference matrix has direct contributions from two subspace projections based on previous inputs, $A_n X_n X_n^H$ and $A_{n-1} X_{n-1} X_{n-1}^H$. More importantly, there is also a contribution from the *complimentary* subspace in the term $\hat{A}_{n-1}(I - X_n X_n^H)$. Most significantly, the expression in (15) can not be reduced such that there is a common subspace projection from the right as in the subspace trap example of (14). This shows that the right singular vectors of $(\tilde{A}_{n+1} - \hat{A}_n)$ will not necessarily be biased toward the previous inputs X_n. Thus, it seems reasonable to predict that using $Y_n X_n^H$ as the predictor input should lead to high-quality estimates without falling into a subspace trap. This conjecture is confirmed empirically in Section V.

V. EXAMPLES

To compare our doubly adaptive temporal update method (DATUM) utilizing a linear predictor (LP), i.e., DATUM-LP, with a collection of low-order dynamic MRI acquisition methods proposed previously, we simulated each method using a dynamic MRI data sequence showing a chop-stick "needle" inserting into a grapefruit. The data was acquired on a 1.5 Tesla GE Signa scanner using a spin-echo sequence to acquire the full 92×92 element k-space data matrix for each of the 30 images in the sequence.

For each image in the original sequence, the grapefruit was pulled from the scanner and the chop-stick inserted slightly farther into the fruit. The fruit was then re-positioned in the scanner and a full k-space data acquisition scan was performed. One side effect of pulling the fruit from the scanner was that the phase orientation of the spins was randomized for each new image. Since

this effect violates our dynamic model assumptions for smoothness, only the magnitude component of the reconstructed image data was used in the simulations below. Obviously, randomization of spin phase will not be a concern in a normal scan sequence. Thus, we fully expect our simulation results presented here to be reproducible in scanner experiments.

In the examples below, we compare the FK, kSVD, and RIGR methods with the DATUM solution using both optimal (DATUM-Opt) and linear predictor guided (DATUM-LP) input selection methods. To briefly review:

- In the FK method, the full k-space data set of the first image in the sequence is acquired, A_0. Each additional image is reconstructed by using only r new lines of k-space, typically associated with the lowest frequency components. An estimate of the k-space data matrix for the new image is constructed by combining the newly acquired data for the low-frequency components with data from the reference image for the high-frequency components. Analytically, this can be described via (7).
- The keyhole SVD method (kSVD) used for comparison in this section uses the same estimate update equation as FK (7). However, in this case, the input vectors X are chosen from the dominant right singular vectors of A_0 rather than the lowest frequency Fourier basis vectors. Note that the input vectors X do not change over the course of the sequence in either the FK or the kSVD methods.
- The RIGR method [11], [30], is an extension of the FK method. The central concept of the method is to identify a linear combination of reference image k-space data that most accurately reflects the acquired phase-encoded data for the most recent image acquisition. The model parameters identified in this first step are then used to estimate the k-space data matrix of the current image.

From [30], the RIGR estimate for r lines of sampled central region k-space data may be written as

$$\hat{A}_n(u, v) = |A_0(u, v)| \circ \sum_{j=-r/2}^{r/2-1} c_j e^{j2\pi j\Delta k u} \qquad (16)$$

where u and v are the indices of the image matrix, c_j are the RIGR model parameters, and $\circ$ is an element-by-element product (also known as the Hadamard or Schur product, [27, Ch. 5]). This estimation step is performed on a row-by-row basis to construct the estimate of the dynamic image. Using the sampled k-space data, $d_n(u, v)$, the model parameters c_j are determined via

$$d_n(m, v) = \sum_{j=-r/2}^{r/2-1} c_j \hat{d}_0(m-j, v), \qquad -r/2 \le m \le r/2-1 \qquad (17)$$

where

$$\hat{d}_0(m-j, v) = \int_{-\infty}^{\infty} |A_0(u, v)| e^{-j2\pi(m-j)\Delta k u}\, du. \qquad (18)$$

This set of equations identifies the model parameters for each image via a best linear fit of the reference data to the most recently sampled data.

- The DATUM-LP method uses the adaptive framework update equation (8) to form the image estimate. New data acquisition vectors are identified by first predicting the next image in the sequence using (12) and then determining the dominant right singular vectors of the difference matrix $(\tilde{A}_{n+1} - \hat{A}_n)$. For the results shown here, the predicted image is constructed from a linear combination of three past image estimates

$$\tilde{A}_{n+1} = \left[4\breve{A}_n + \breve{A}_{n-1} - 2\breve{A}_{n-2}\right] \Big/ 3$$

where the predictor input is the low-rank estimate, $\breve{A}_n = Y_n X_n^H$.
- The theoretically optimal method (DATUM-Opt) uses the adaptive framework update equation (8) to form the image estimate. New data acquisition vectors are selected from the dominant right singular vectors of the difference between $(A_{n+1} - \hat{A}_n)$ using the actual image sequence. Note that because complete knowledge of each image in the sequence is required, this technique is not realizable in a clinical setting. It is shown here to provide a sense of the possible performance available with the DATUM approach.

For each of these methods, the first image in the sequence was used for the reference image. For the DATUM-LP method, zero matrices were used at the start of the sequence at those times where previous image estimates where unavailable, e.g., $\tilde{A}_1 = (4/3)A_0 + (1/3)\mathbf{0} - (2/3)\mathbf{0}$. For each of the examples below, the number of input vectors r used for each low-order data acquisition was chosen such that 99.5% of the reference image information is captured in an SVD low-rank reconstruction. Specifically, $r = t$ such that $\sum_{i=1}^{t} \sigma_i^2 / \sum_{i=1}^{N} \sigma_i^2 = 0.995$, where $\{\sigma_i\}$ are the singular values of the reference image A_0.

A. Full Grapefruit Sequence

The first example shows the acquisition simulation results for the entire grapefruit sequence data using $r = 25$ input vectors. With the original image 92×92 pixels in size, this value for r corresponds to an acquisition time of 27% of the time required for acquiring the complete k-space data set. Stated a different way, by using $r = 25$ input vectors almost four low-order estimates could be reconstructed in the same time as one full data image acquired via traditional Fourier encoding.

Fig. 1 compares the relative error, $\sqrt{\mathcal{E}_n}/\|A_n\|_F$, for each of the low-order methods: FK, kSVD, RIGR, DATUM-LP, and DATUM-Opt. As can be seen in Fig. 1, the static input methods, FK, kSVD, and RIGR, all show similar performance. Choosing the input vectors dynamically via the DATUM-LP method provides significant improvement compared to each of these static input methods. Furthermore, while the performance of the static input methods steadily deteriorates over time, our doubly adaptive method maintains a much lower level of error as the sequence progresses. The relative error in the static input estimates is proportional to the deviation of the current true image from the reference image. In contrast, our doubly adaptive method shows small variations around a much lower steady state error level. Notice as well that there is still a significant difference in the relative error between the realizable DATUM-LP method and the theoretical bound given by the nonrealizable optimal method, DATUM-Opt.

These observations are confirmed by visual inspection of Figs. 2–6. In each of these figures, the estimate sequence

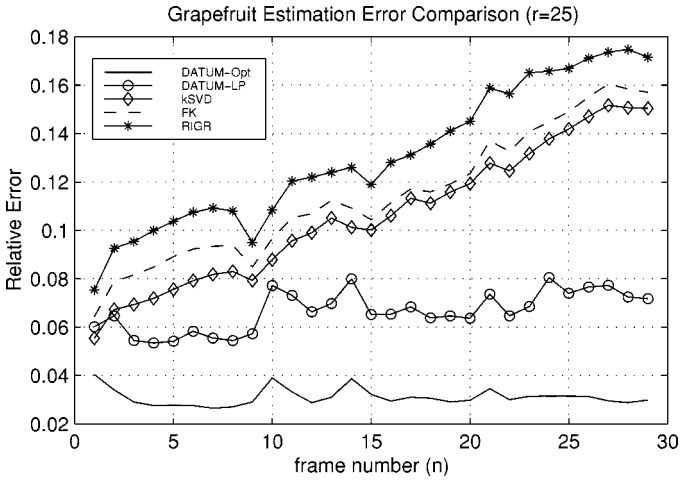

Fig. 1. Relative error comparison, $\sqrt{\mathcal{E}_n}/\|A_n\|_F$, between the dynamic sequence estimation methods for the full grapefruit data set example.

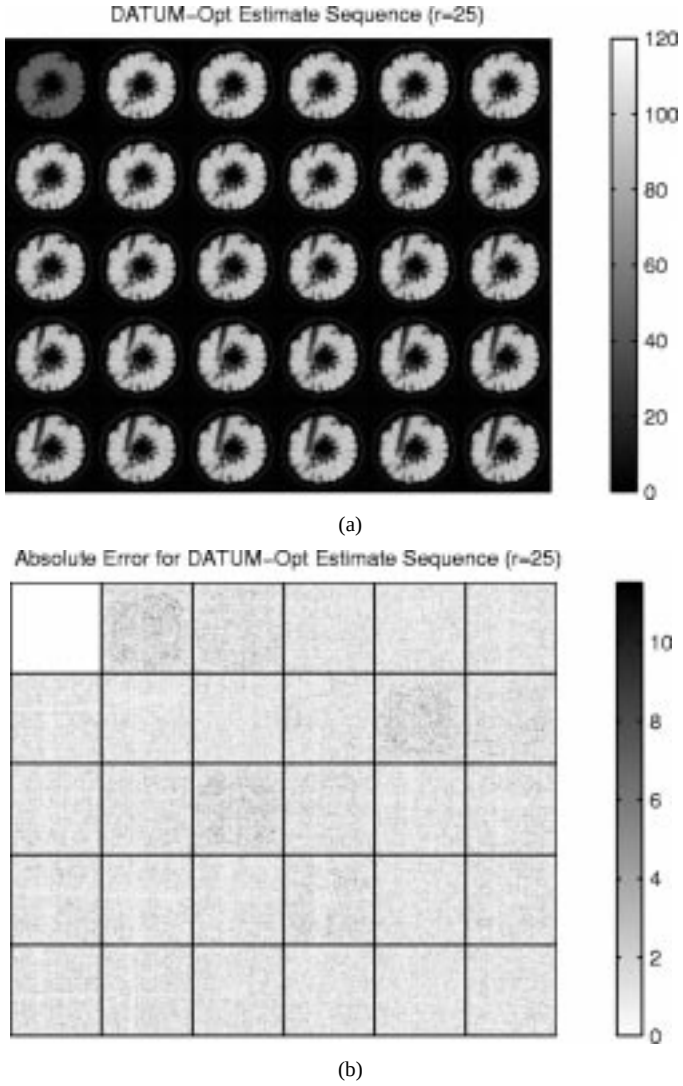

Fig. 2. DATUM-Opt estimate and estimate error of a simulated grapefruit data acquisition using $r = 25$ input acquisition vectors. Each image is 92×92 pixels in size and the time sequence moves left-to-right and top-to-bottom with the original (shaded) reference image in the upper left corner.

is given in (a) and absolute error sequence is given in (b). These figures show each sequence with time advancing first left-to-right, and then top-to-bottom. That is, the top left image is associated with $n = 0$, the top right image is associated with $n = 5$, and the bottom right image is associated with $n = 29$.

The results of DATUM-Opt, Fig. 2, show a high-quality sequence estimate with a low maximum pixel error compared to the other methods. The most significant difference between Fig. 2(b) and the estimate error of the static input methods, i.e., FK, RIGR, and kSVD, shown in Figs. 3(b), 4(b), and 5(b) respectively, is that the error images of the optimal method are not spatially correlated with the structure of the image estimate. In contrast, the absolute error images of the static input methods appear to be almost an outline of the high-intensity signal regions of the fruit. This indicates a slight bulk motion shift of the fruit over the course of sequence. In particular, Fig. 4 shows that the RIGR method is unable to accurately estimate such bulk motion. This is due to the applied spatial reference envelope formed from the intensity values of the reference image which is a key component of the RIGR method. Notice as well that there appears to be significant blurring of the chop-stick edges in the FK sequence, and significant artifacts at the edges of the fruit in the kSVD estimated sequence.

Notably, these artifacts are mostly absent from the DATUM-LP estimate, Fig. 6. Furthermore, Fig. 6(b) illustrates that the linear prediction method estimate error also has significantly less structural correlation with the image sequence than the static input methods. Note that the scale of the error images is comparable to the kSVD method. However there are only a few pixels that approach the maximum error value, notably in the error images in the first column at $n = 6$ and $n = 21$. While the results of this method approach the high-quality available in the optimal method, Fig. 2(b), the peak error level is higher and the structural correlation between the error and the image is stronger.

B. Bulk Motion Simulation

To demonstrate the ability of the doubly adaptive methods to track significant object motion in an image sequence, the example here focuses on the region exhibiting the most change in the previous example. The image set used in this example utilizes a smaller field of view (FOV), 32×32 pixels in size, centered on the upper left quadrant of the fruit. The number of images in the sequence was reduced to 9 to allow greater visible detail in the figures. Furthermore, to simulate bulk motion in the phantom, the FOV was spatially shifted at frame $n = 3$ by one pixel in both the horizontal and vertical direction. Each of the minimal data dynamic MRI methods discussed in the previous example were simulated with this data set using $r = 9$ input vectors.

The relative error comparison, Fig. 7, shows that all of the sequence estimation methods suffer a loss in quality at the third estimate, corresponding to the simulated bulk motion shift of the FOV at $n = 3$. However, only the doubly adaptive methods, DATUM-LP and DATUM-Opt, are able to recover after the shift and continue tracking. Note that their level of error after the shift point gradually declines toward its pre-shift value. In particular, the error in the DATUM-Opt method is on the same order as

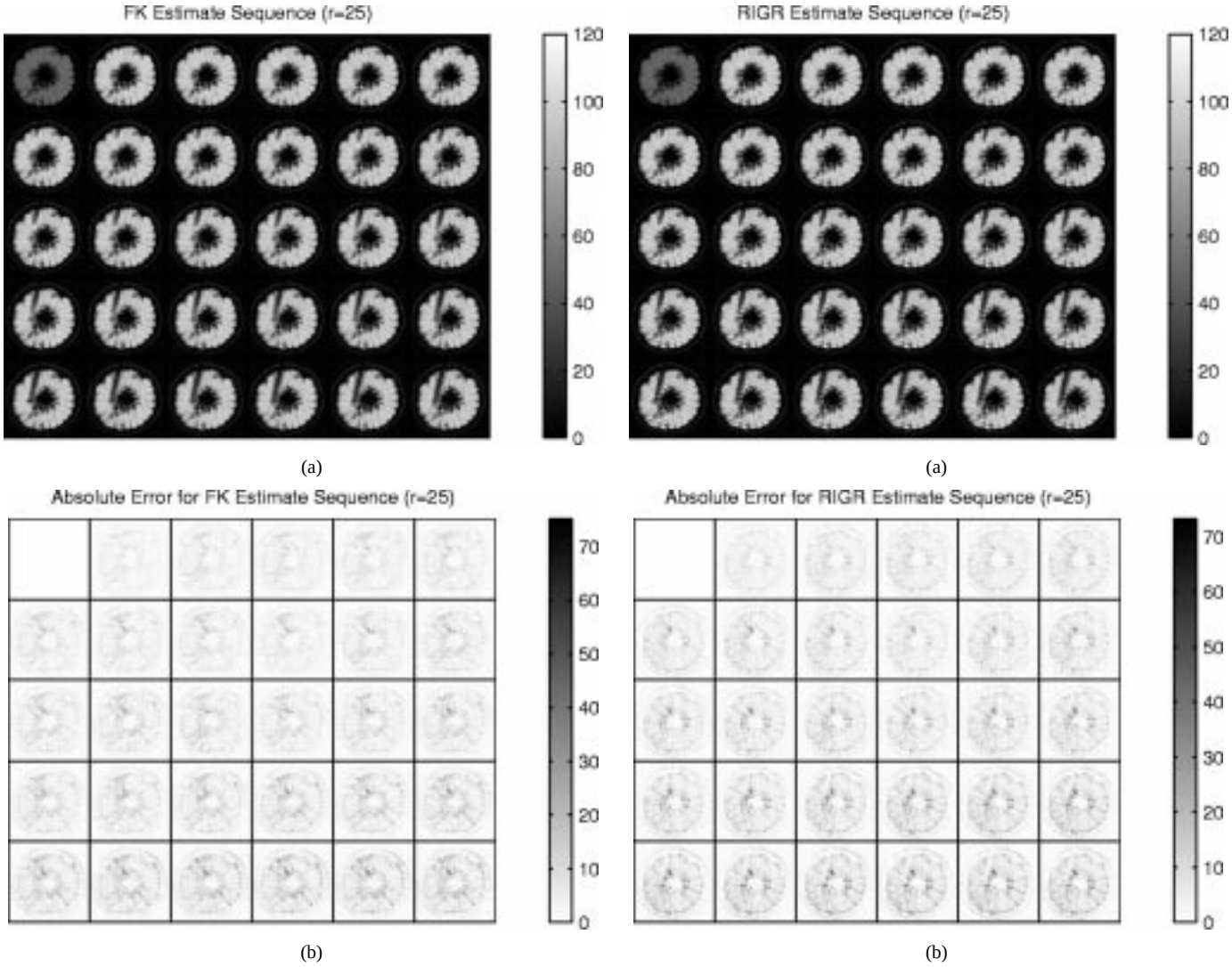

Fig. 3. FK estimate and estimate error sequences. Figure layout as in Fig. 2.

Fig. 4. RIGR estimate and estimate error sequences. Figure layout as in Fig. 2.

before the shift after only a few frames. In contrast, the static methods never recover after the shift point.

Figs. 8 and 9 show the estimates and the absolute estimate error for the eight estimated images of the shifted FOV sequence. Each column shows eight frames of a particular estimate method. Again, the DATUM-Opt method provides a very high-quality estimate over the entire sequence. The quality shown is the theoretical limit for the doubly adaptive method, and clearly indicates that if one could accurately predict bulk motion changes then high-quality estimates are available with a very limited amount of data.

Consistent with the first example, these figures also show significant artifacts in the static input methods: FK, kSVD, and RIGR. As these methods were originally billed as contrast change estimation methods, this is not unexpected. In contrast, Fig. 9 shows that the doubly dynamic input methods, DATUM-Opt and DATUM-LP, contain significantly less error that is correlated to the structure of the reference image and the absolute error shows a decrease across the entire FOV after the shift point. From Fig. 8, we also note that the "ringing" artifacts present in the static input methods are notably absent in the doubly adaptive methods.

C. Concluding Remarks

These examples show that adaptively tailoring the input vectors for each successive image in a sequence can provide a significant improvement in estimation of the sequence. The first example demonstrated the applicability of the method for a representative clinical sequence. The second example showed that the method may even be able to reasonably estimate sequences with significant changes, such as that introduced by a bulk motion change in the FOV. The biggest advantage of the doubly adaptive method demonstrated in these examples is the ability for the image estimate to recover within a few frames after a significant change, even if it may not perform better than the static input methods for a particular frame, as in the second example at $n = 3$.

VI. Discussion and Summary

In this paper, we have presented an adaptive framework for the estimation of dynamic MRI sequences. This framework was shown to be a general form which could also describe analytically the previous FK and SVD acquisition methods under certain assumptions. Because the framework was developed using

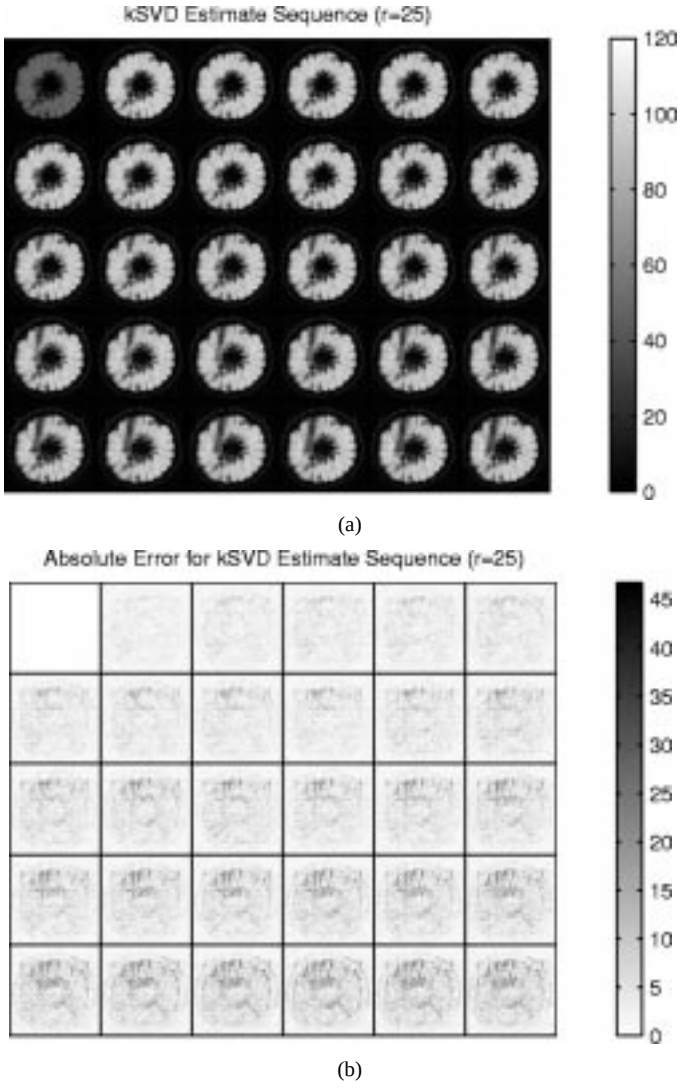

Fig. 5. kSVD estimate and estimate error sequences. Figure layout as in Fig. 2.

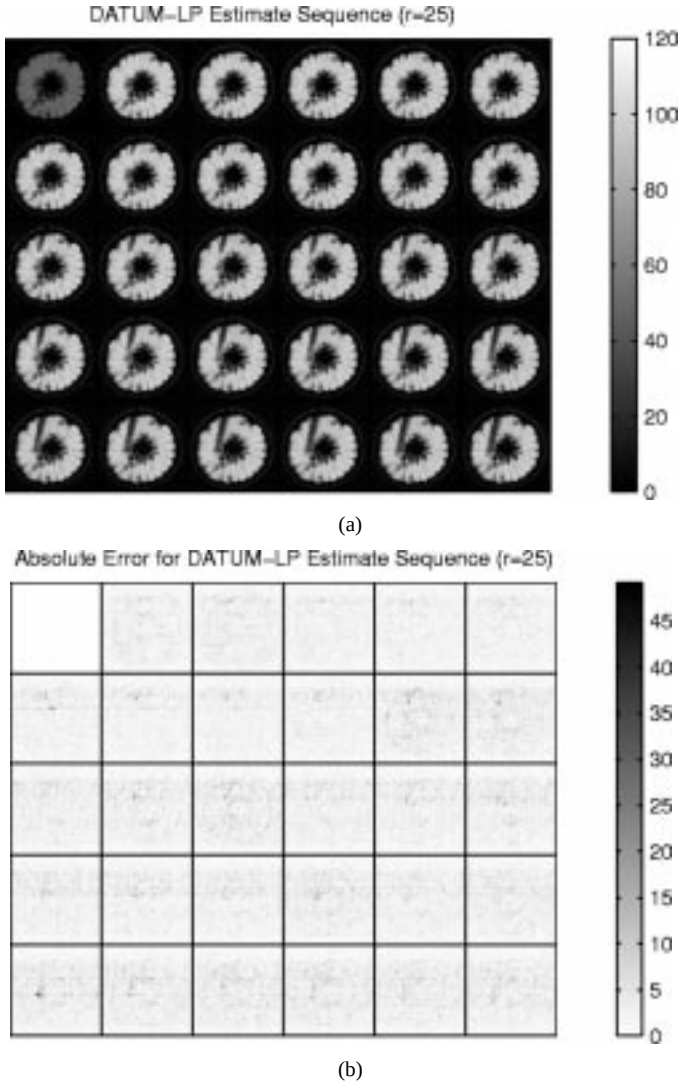

Fig. 6. DATUM-LP estimate and estimate error sequences. Figure layout as in Fig. 2.

concepts drawn from adaptive filter theory, it also shows a resemblance to the LMS adaptive filter structure, and we expect it to be applicable for any tracking or system estimation problem where one has complete control of the inputs and the linear system model applies.

The computational requirements of the proposed algorithm are not significantly greater than those in the original SVD acquisition method. As in the SVD methods, the dominant right singular vectors of a matrix must be determined with each new estimate. This can be computed efficiently using such algorithms as the conjugate gradient SVD [31]. The additional computational requirements are only four accumulates per pixel. In fact, the only significant cost beyond that of the original SVD method is the memory required to store the delay chain of the predictive filter.

At first glance, it may appear that rf or spatially selective encoding suffers from low SNR when compared to Fourier acquisition methods because only a portion of the spins in the FOV are excited as opposed to the entire FOV. However, the increased image information acquisition rate provided by spatially selective encoding methods can quickly overcome this difficulty. For example, in the case of wavelet excitations, is was shown in [32] that the relative estimation error of an image is potentially much lower given a limited number of wavelet acquisition vectors than a comparable limited amount of Fourier acquired data.

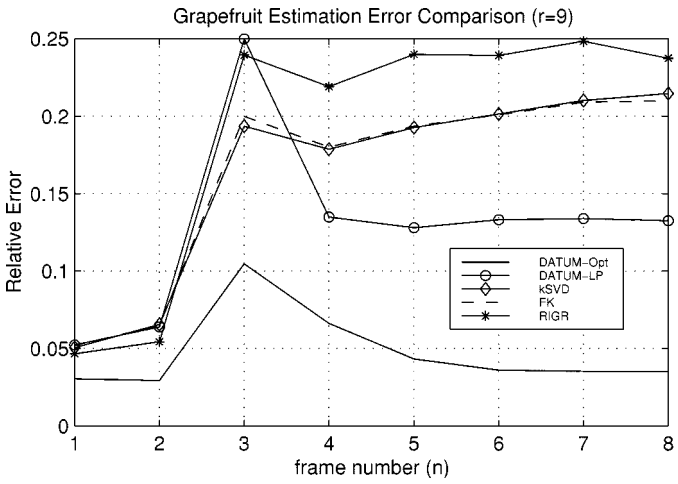

Fig. 7. Relative error comparison, $\sqrt{\mathcal{E}_n}/\|A_n\|_F$, between dynamic MRI sequence estimation methods for the limited FOV with bulk motion example.

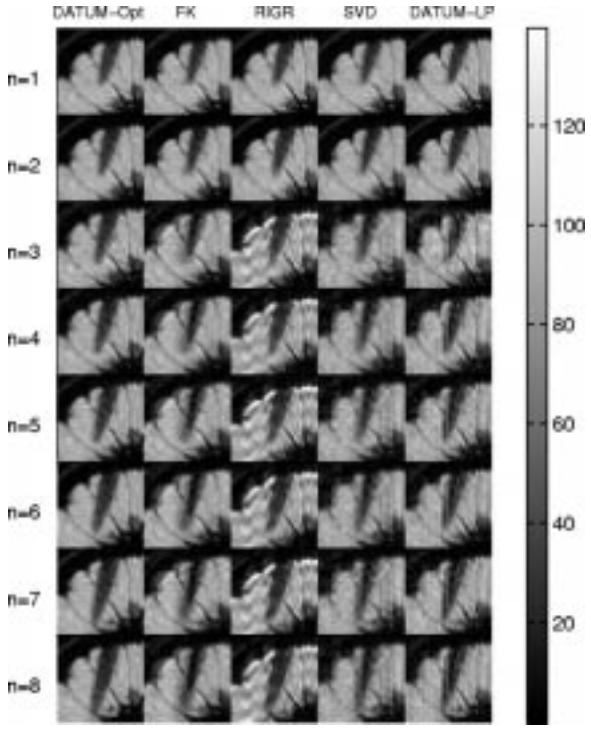

Fig. 8. Comparison of image estimates for shifting FOV sequence. Each column contains eight sequential image estimates produced by the method listed at the top of the column.

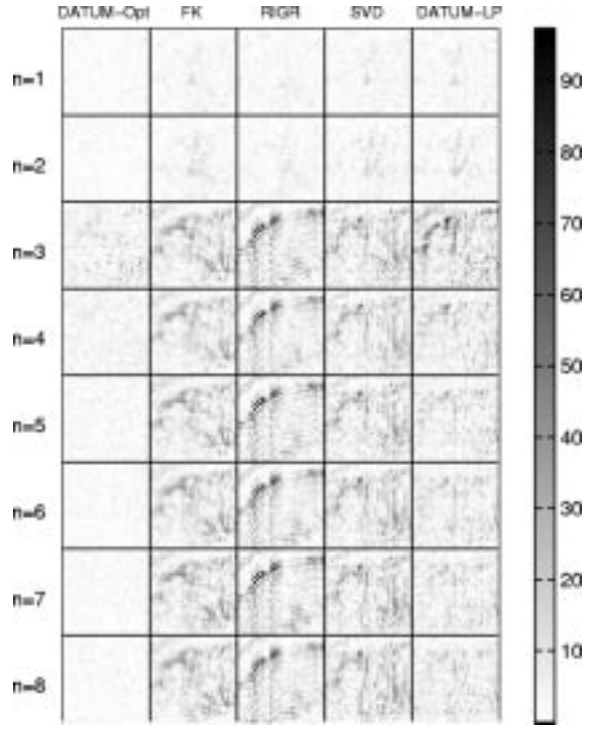

Fig. 9. Estimate error comparison for shifting FOV sequence. Layout as in Fig. 8.

So while the received rf signal from say 16 non-Fourier based input vectors in a spatially selective encoding MR protocol may suffer from lower SNR per encode, if the non-Fourier inputs are chosen carefully the reconstructed image will typically have much lower estimate error than the dominant 16 Fourier acquired vectors of the same FOV.

Finally, we are currently working to address a number of remaining issues before this method can be used in a practical setting. For one, we have assumed here that the input vectors can be chosen arbitrarily and with equal time between each input. Depending on the imaging protocol used, it may in fact be advantageous to instead use a constrained input vector set such as the pseudo-SVD-style vectors proposed in [33].

In addition, the linear system model in (1) assumes that the system has no memory between successive inputs, i.e., the spins completely relax before each input excitation. This is the worst case scenario for a direct SNR comparison between Fourier and non-Fourier encoding. However, at the other extreme, for modalities where there is no relaxation, e.g., hyper-polarized gas imaging, it can be shown [34] that all orthogonal input bases have equivalent SNR response. Practical MR imaging in fact lies somewhere between these two extremes of "complete relaxation" and "no relaxation" of the bulk magnetization.

In our analysis of the adaptive framework estimate error, we showed that having complete knowledge of the next image in the sequence will provide an optimal set of data acquisition vectors. Because such knowledge is not available in practice, we proposed using the output of a linear predictor to determine appropriate data acquisition vectors. Examples of simulated sequence acquisitions using real MRI data were given showing that such a strategy provides significant improvement compared to other well known minimum data image sequence acquisition techniques. Moreover, the difference in performance between the realizable methods and the theoretically optimal method indicates that room for improvement still exists. Improving the performance of the realizable methods via alternative linear predictors is a focus of current research.

REFERENCES

[1] J. Tacke, G. Adam, H. Classen, A. Muhler, A. Prescher, and R. W. Gunther, "Dynamic MRI of a hypovascularized liver tumor model," *J. Magn. Reson. Imag.*, vol. 7, pp. 678–682, July–Aug. 1997.

[2] F. Wallis and F. J. Gilbert, "Magnetic resonance imaging in oncology: An overview," *J. R. Coll. Surg. Edinb.*, vol. 44, pp. 117–125, Apr. 1999.

[3] F. A. Jolesz and S. M. Blumenfeld, "Interventional use of magnetic resonance imaging," *Magn. Reson. Q*, vol. 10, pp. 85–96, June 1994.

[4] P. C. Yang, A. B. Kerr, A. C. Liu, D. H. Liang, C. Hardy, C. H. Meyer, A. Macovski, J. M. Pauly, and B. S. Hu, "New real-time interactive cardiac magnetic resonance imaging system complements echocardiography," *J. Am. Coll. Cardiol.*, vol. 32, pp. 2049–2056, Dec. 1998.

[5] A. B. Kerr, J. M. Pauly, B. S. Hu, K. C. Li, C. J. Hardy, C. H. Meyer, A. Macovski, and D. G. Nishimura, "Real-time interactive MRI on a conventional scanner," *Magn. Reson. Med.*, vol. 38, pp. 355–367, Sept. 1997.

[6] G. A. Wright, "Magnetic resonance imaging," *IEEE Signal Processing Mag.*, vol. 14, pp. 56–66, Jan. 1997.

[7] Z.-P. Liang and P. C. Lauterbur, *Principles of Magnetic Resonance Imaging: A Signal Processing Perspective*. New York: IEEE Press, 1999.

[8] P. T. Callaghan, *Principles of Nuclear Magnetic Resonance Microscopy*. New York: Oxford Univ. Press, 1991.

[9] D. K. Sodickson and W. J. Manning, "Simultaneous acquisition of spatial harmonics (SMASH): Fast imaging with radio frequency coil arrays," *Magn. Reson. Med.*, vol. 38, no. 4, pp. 591–603, Oct. 1997.

[10] J. van Vaals and M. E. Brummer *et al.*, "Keyhole method for accelerating imaging of a contrast agent uptake," *J. Magn. Reson. Imag.*, vol. 3, no. 4, pp. 671–675, July/Aug. 1993.

[11] Z.-P. Liang and P. C. Lauterbur, "An efficient method for dynamic magnetic resonance imaging," *IEEE Trans. Med. Imag.*, vol. 13, pp. 677–686, Dec. 1994.

[12] S. K. Nagle and D. N. Levin, "Multiple region MRI," *Magn. Reson. Med.*, vol. 41, no. 4, pp. 774–786, Apr. 1999.

[13] D. M. Healy, Jr. and J. B. Weaver, "Two applications of wavelet transforms in magnetic resonance imaging," *IEEE Trans. Inform. Theory*, vol. 38, pp. 840–860, Mar. 1992.
[14] L. P. Panych, P. D. Jakab, and F. A. Jolesz, "An implementation of wavelet encoded MRI," *J. Magn. Reson. Imag.*, vol. 3, p. 649, 1993.
[15] L. P. Panych, C. Oesterle, G. P. Zientara, and J. Henning, "Implementation of a fast gradient-echo SVD encoding technique for dynamic imaging," *J. Magn. Reson. Imag.*, vol. 35, pp. 554–562, Apr. 1996.
[16] L. P. Panych, P. Saiviroonporn, G. P. Zientara, and F. A. Jolesz, "Implementation of a 3D echo-planar method for SVD encoded MRI," in *Proc. ISMRM 4th Scientific Meeting*, New York, 1996, p. 387.
[17] D. Mitsouras, A. S. Edelman, L. P. Panych, F. A. Jolesz, and G. P. Zientara, "Fast multiple-excitation multiple-echo spin-echo pulse sequence for non-Fourier spatial encoding," in *Proc. ISMRM 9th Scientific Meeting*, Glasgow, U.K., Apr. 2001, p. 1808.
[18] S. J. Reeves and Z. Zhao, "Sequential algorithms for observation selection," *IEEE Trans. Signal Processing*, vol. 47, pp. 123–132, Jan. 1999.
[19] P. J. Bones, N. Alwesh, T. J. Connolly, and N. D. Blakeley, "Recovery of limited-extent images aliased because of spectral undersampling," *JOSA A*, vol. 18, pp. 2079–2088, Sept. 2001.
[20] L. P. Panych, G. P. Zientara, and F. A. Jolesz, "MR image encoding by spatially selective rf excitation: An analysis using linear response models," *Int. J. Imag. Syst. Technol.*, vol. 10, no. 2, pp. 143–150, 1999.
[21] D. M. Healy and J. B. Weaver, "Adapted waveform encoding for magnetic resonance imaging," *IEEE Eng. Med. Biol. Mag.*, vol. 14, pp. 621–638, Sept. 1995.
[22] A. K. Jain, *Fundamentals of Digital Image Processing*. Englewood Cliffs, NJ: Prentice-Hall, 1989.
[23] G. P. Zientara, L. P. Panych, and F. A. Jolesz, "Dynamically adaptive MRI with encoding by singular value decomposition," *Magn. Reson. Med.*, vol. 32, pp. 268–274, Aug. 1994.
[24] G. P. Zientara, L. P. Panych, and F. A. Jolesz, "Keyhole SVD encoded MRI," in *Proc. SMR 2nd Annu. Meeting*, San Francisco, CA, 1994, p. 778.
[25] R. A. Horn and C. R. Johnson, *Matrix Analysis*. New York: Cambridge Univ. Press, 1985.
[26] S. Haykin, *Adaptive Filter Theory*, 3rd ed. Englewood Cliffs, NJ: Prentice-Hall, 1996.
[27] R. A. Horn and C. R. Johnson, *Topics in Matrix Analysis*. New York: Cambridge Univ. Press, 1991.
[28] G. Hämmerlin and K.-H. Hoffmann, *Numerical Mathematics*. Berlin, Germany: Springer-Verlag, 1991.
[29] W. S. Hoge, "An adaptive signal processing approach to dynamic magnetic resonance imaging," Ph.D. dissertation, Northeastern Univ., Boston, MA, June 2001.
[30] J. M. Hanson, Z.-P. Liang, R. L. Magin, J. L. Duerk, and P. C. Lauterbur, "A comparison of RIGR and SVD dynamic imaging methods," *Magn. Reson. Med.*, vol. 38, pp. 161–167, July 1997.
[31] G. H. Golub and C. F. Van Loan, *Matrix Computations*, 3rd ed. Baltimore, MD: Johns Hopkins Univ. Press, 1996.
[32] L. P. Panych, "Theoretical comparison of Fourier and wavelet encoding in magnetic resonance imaging," *IEEE Trans. Med. Imag.*, vol. 15, pp. 141–153, Apr. 1996.
[33] ——, "Partial non-Fourier encoding," in *Proc. ISMRM Minimum MR Data Acquisition Methods Workshop*, Marco Island, FL, Oct. 2001, pp. 62–65.
[34] L. Zhao, A. K. Venkatesh, M. S. Albert, and L. P. Panych, "Signal-to-noise ratio comparison of encoding methods for hyperpolarized noble gas MRI," *J. Magn. Reson.*, vol. 148, pp. 314–326, Feb. 2001.

William Scott Hoge (S'98–M'02) received the B.A. degree in physics from Colorado College, Colorado Springs, in 1991, and the M.S. and Ph.D. degrees in electrical engineering from Northeastern University, Boston, MA, in 1994 and 2001, respectively.

From 1994 to 1997, he was a DSP Engineer with Natural Microsystems, Framingham. He is currently a Research Fellow at Brigham and Women's Hospital, Boston. His current research is focused on applying adaptive filtering, system identification, and subspace optimization concepts to magnetic resonance imaging. His research interests include adaptive filters, image, and audio signal processing.

Eric L. Miller (S'90–M'95) received the S.B. degree in 1990, the S.M. degree in 1992, and the Ph.D. degree in 1994 all in electrical engineering and computer science from the Massachusetts Institute of Technology, Cambridge.

He is currently an Associate Professor in the Department of Electrical and Computer Engineering at Northeastern University, Boston, MA. His research interests include the use of multiscale and statistical methods for the solution of inverse problems in general and inverse scattering problems in particular and the development of computationally efficient, physically based models for use in applications such as mine detection, target recognition, medical imaging, and environmental monitoring and remediation.

Dr. Miller is a member of Tau Beta Pi, Eta Kappa Nu, and Phi Beta Kappa and received the CAREER Award from the National Science Foundation in 1996. He is currently serving as an Associate editor for the IEEE TRANSACTIONS ON IMAGE PROCESSING.

Hanoch Lev-Ari (S'78–M'84–SM'93) received the B.S. degree (summa cum laude) in 1971 and the M.S. degree in 1978, both in electrical engineering from the Technion—Israel Institute of Technology, Haifa, and the Ph.D. degree in electrical engineering from Stanford University, Stanford, CA, in 1984.

He is currently an Associate Professor with the Department of Electrical and Computer Engineering at Northeastern University. His present areas of interest include model-based spectrum analysis and estimation for nonstationary signals, scale-recursive (multirate) detection and estimation of random signals, and adaptive linear and nonlinear filtering techniques, with applications to channel equalization, over-the horizon (OTH) radar, automatic target detection and recognition, and identification of time-variant systems. He served as an Associate Editor of *Circuits, Systems and Signal Processing* and *Integration, the VLSI Journal*.

Dr. Lev-Ari is a member of SIAM.

Dana H. Brooks (S'86–M'91) received the B.A. degree in English in 1972 from Temple University, Philadelphia, PA, the B.S.E.E. degree in 1986, the M.S.E.E. degree in 1988, and the Ph.D. degree in 1991, all in electrical engineering, from Northeastern University, Boston, MA.

He is an Associate Professor of electrical and computer engineering, Associate Director of the Center for Communications and Digital Signal Processing, a Member of the Center for Subsurface Sensing and Imaging Systems, and PI of the Biomedical Signal Processing Laboratory, Northeastern University. His research interests are in statistical and digital signal processing, with particular application to biomedical problems and image sequence processing.

Dr. Brooks is an Associate Editor and Member of the Editorial Board of *IEEE Signal Processing Magazine*.

Lawrence P. Panych received the B.S. and M.S. degrees in electrical engineering from McGill University, Montreal, QC, Canada, and the University of British Columbia, Vancouver, BC, Canada, respectively, and the Ph.D. degree in radiological sciences from the Massachusetts Institute of Technology, Cambridge, in 1993.

He is an Associate Professor of radiology at Brigham and Women's Hospital, Boston, MA, and Harvard Medical School, Cambridge, MA, and is active in the development of new methods in magnetic resonance imaging. His major area of research is in the development of real-time adaptive methods for dynamic MRI. He specializes in development of image encoding methods using spatially selective RF encoding, sometimes also referred to as non-Fourier encoding.